RESEARCH ARTICLE



Detonation cell size estimation via chemiluminescence imaging in an optically accessible linear detonation tube

Brandon M. Ng¹ · Eugene N. A. Hoffman¹ · Daniel I. Pineda¹ · Christopher S. Combs¹

Received: 23 February 2024 / Revised: 3 June 2024 / Accepted: 22 June 2024 / Published online: 5 July 2024 © The Author(s), under exclusive licence to Springer-Verlag GmbH Germany, part of Springer Nature 2024

Abstract

An optically based experimental approach for estimating detonation cell size of premixed gas phase fuel—oxidizer mixtures in an optically accessible linear detonation tube is presented. Detonation wave fronts propagating through undiluted near-stoichiometric ethylene—oxygen mixtures in the circular detonation tube were visualized and recorded using CH* chemiluminescence imaging near 430 nm at 100 kHz for initial mixture pressures up to 22 kPa. The chemiluminescence imaging, coupled with high-speed videography, is shown to capture cellular detonation structures as small as 1.6 mm in width. The measured cell sizes increase as the initial fill pressure decreases, corroborating well-established relationships between detonation cell sizes and initial reactant pressures. The optically based method is validated against conventional soot foil measurements performed simultaneously with multiple detonations at various initial fill conditions. Both chemiluminescence images and soot foil measurements are compared to previously published cell size trends for undiluted fuel—oxygen detonations, demonstrating reasonable agreement with the established methods. Paired with the optically accessible detonation channel, the high-speed chemiluminescence imaging technique offers a passive estimation of detonation cell size for the range of conditions investigated with a faster experimental turnaround time relative to conventional methods.

1 Introduction

Detonation combustion has gained growing interest in recent decades for both propulsion and energy applications due to its theoretical thermodynamic advantages and potential for mechanical simplicity relative to conventional thermodynamic cycles and systems (Wolański 2013; Heiser and Pratt 2008). This is especially so for chemical propulsion systems such as pulse detonation engines (PDEs) and rotating detonation engines (RDEs), where high combustion performance, high cycle efficiency, and a lower system mass are desirable (Lu and Braun 2014). To study detonations and their thermochemical properties in a controlled and repeatable manner, impulse facilities such as detonation tubes are often used. However, owing to extreme pressures and temperatures produced by detonation combustion, these facilities typically have limited optical access, restricting visualization characterization to only portions of the flow

Here, to address these challenges associated with planar geometries, we leverage a thick acrylic tube to visualize the detonation wave as it propagates through the channel. The optically accessible section enables implementation of high-speed visualization techniques with large viewing areas at both visible and near-UV wavelengths that would otherwise be difficult in small-diameter metal circular detonation channels.

In the present study, chemiluminescence imaging—commonly used to visualize flames (Liu et al. 2020; Cadman et al. 2002)—is applied as a method of observing the detonation wave structure and estimating detonation cell size (DCS), a fundamental length parameter used to predict detonation behavior and an important characteristic in the design



accessible through small-diameter optical probes or windows. Detonation tubes with optical access to the full flow field typically have planar configurations (Radulesco et al. 2007; Kellenberger and Ciccarelli 2015), which simplifies the optical setup, but limits the allowable detonation pressures to regimes which are far lower than those observed in practical detonation combustion devices. Planar configurations also create multi-dimensional nonuniformities in the boundary layer, posing difficulties for comparison to simplified and more computationally tractable detonation models.

[☐] Daniel I. Pineda daniel.pineda@utsa.edu

Department of Mechanical Engineering, The University of Texas at San Antonio, 1 UTSA Circle, San Antonio, TX 78249, USA

of detonation engines. As an integrated line-of-sight technique, chemiluminescence imaging has been used by multiple researchers to study detonations (Bennewitz et al. 2019; Fugger et al. 2020; Nair et al. 2023; Frederick et al. 2023, 2022; Rankin et al. 2017; Gray and Lacoste 2021; Chatelain et al. 2023), sometimes in conjunction with planar laserinduced fluorescence (PLIF) to resolve the reacting flow field structures in specific locations (Ayers et al. 2022; Athmanathan et al. 2022; Lemcherfi et al. 2023; Rojas Chavez et al. 2023) or simultaneously with schlieren imaging to also obtain information about the density field (Frederick et al. 2023, 2022). Owing to its applicability to detonations fueled by hydrogen, hydrocarbons, and nitrogen-based propellants, broadband (Bennewitz et al. 2019; Fugger et al. 2020; Nair et al. 2023; Frederick et al. 2023) and OH* (Frederick et al. 2022; Rankin et al. 2017; Gray and Lacoste 2021; Chatelain et al. 2023; Ayers et al. 2022; Athmanathan et al. 2022; Lemcherfi et al. 2023; Rojas Chavez et al. 2023) chemiluminescence have been most frequently used, with OH* chemiluminescence typically requiring a UV intensifier to capture spontaneous emission near 309 nm since this wavelength is outside the sensitive range of most high-speed cameras. CH* chemiluminescence has been less commonly used, but offers a larger dynamic range with which to analyze detonation structures generated by carbon-containing fuels (Frederick et al. 2022).

Traditionally, cell size has been experimentally determined through soot foil (or smoked soot) measurements (Lee 2008; Zhang 2012). In this technique, a soot-covered surface is placed in the detonation channel where it is exposed to the reacting flow, typically on the wall. As the detonation passes over the soot-covered surface, the wave front displaces the soot, leaving behind an imprint of one or more shock wave interactions in the flow. This region behind the wave front is characterized by multiple shock waves that intersect, as shown in Fig. 1.

The intersections of these shock waves are known as triple points. As the detonation wave propagates, these triple points trace their path onto the soot. The resulting surface is characterized by a series of diamond-shaped patterns. The width of these diamond shapes or cells is known as detonation cell size—commonly denoted by λ . Although repeatable and reliable, soot foil measurements are experimentally time consuming due to the preparation and installation of the soot-covered surface. The objective of this study is to further expand on previous chemiluminescence studies and provide an approach for estimating detonation cell size using CH* chemiluminescence with quicker experimental turnaround times relative to conventional soot foil methods. CH* chemiluminescence also provides a simpler and faster optical setup compared to OH* chemiluminescence, which typically requires the addition of a UV intensifier or photomultiplier tube (Frederick et al. 2022). Lastly, the large viewing

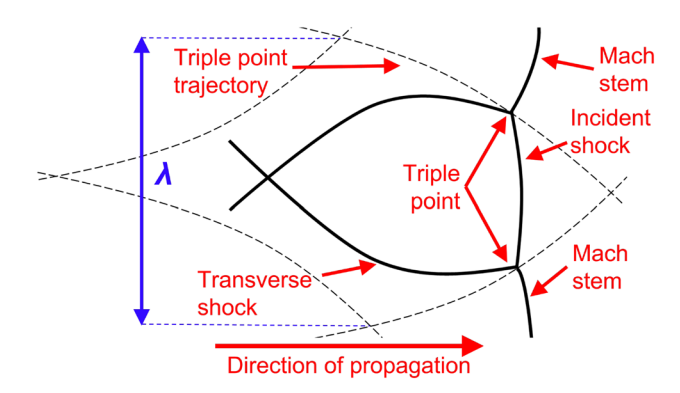


Fig. 1 Detonation wave structure diagram

area offered by the optically accessible configuration readily enables employment of spectral analysis techniques on the recorded images, providing for automated determination of detonation cell sizes observed with chemiluminescence.

2 Experimental methods

Here, we describe the impulse facility used to produce detonation waves, and the corresponding optical setup and methods are used to collect and process the measurement data. We first note that caution should be exercised when handling and mixing propellants, particularly those involving pure oxygen as the oxidizer, and that attention should be paid to the maximum allowable operating pressure of the impulse facility based on its constituent materials (e.g. acrylic, stainless steel) and wall thickness. All experiments shown in this study were performed remotely, with concrete barriers between the operators and the impulse facility.

2.1 Optically accessible detonation tube

For this study, detonations were conducted in a mixture of gas phase ethylene and oxygen (C_2H_4 and O_2 , respectively) with a fuel–oxidizer equivalence ratio of $\phi=1.1$ and constant initial temperature $T_0=296$ K. Initial mixture pressures P_0 ranged from 8.66 to 22.04 kPa.

The design of the linear detonation tube facility at The University of Texas at San Antonio comprises three main sections: (1) the ignition section, (2) the acrylic visual section, and (3) the instrumentation section. These sections are mated together using weldless flanges (Aul et al. 2013) and are constructed with a continuous channel with an inner diameter of 38.1 mm (1.5 inches) and a wall thickness of 12.7 mm (0.5 inches). This type of modular design, which has been successfully leveraged to develop novel detonation diagnostic techniques (Nair et al. 2020, 2023), enables modification of one or more sections to accommodate a wide



range of detonation studies. Downstream of the detonation tube is a multi-purpose 6.06 m³ vacuum tank that allows for rapid and safe expansion and cooling of the detonation product gases after each experiment. A single vacuum pump (Sogevac SV65B) is used for both the detonation tube and vacuum tank. The detonation tube and vacuum tank are separated by a mylar diaphragm to contain the reactant gases while the tube is filled. This diaphragm bursts upon contact with the detonation wave at the end of the experiment, depressurizing the system.

The ignition section, which contains the reactant inlet, is constructed from 304 stainless steel tubing, chosen for its toughness and corrosion resistance. The mixture is ignited by an automotive spark plug located on the end wall of the ignition section. Flow rates for the fuel—oxidizer mixture are regulated by mass flow controllers (Alicat MS-Series) which also measure the initial temperatures of the reactants. Initial pressure within the detonation tube is also measured from the gas manifold with a digital pressure gauge (Ashcroft 2074). A schematic of the detonation tube and the gas manifold used for mixture preparation are depicted in Fig. 2.

The combustion reaction undergoes a deflagration-to-detonation transition (DDT) via the aid of a Shchelkin spiral (New et al. 2006) with a length-to-diameter ratio of 9.6, and a blockage ratio (d/λ) of 46. To view the reacting flow field inside the detonation tube, the visual section comprises a portion of cast acrylic tubing which is transparent in the visible spectrum. The acrylic material was chosen for its optical clarity for the wavelengths targeted in this study, compatibility with several fuel types, and cost-effectiveness. The weldless flanges connecting the visual section to the

other sections of the detonation tube feature face seals with O-ring grooves only on the metal ignition and instrumentation sections; this facilitates interchangeability of the visual section to encompass multiple types of optically transmissible materials for different projects. This optical accessibility allows for high-speed imaging of the reaction and its time evolution as it travels down the detonation tube. To date, more than 30 detonations have been performed through the optical section; inevitably, as the detonation waves cloud the inner acrylic surface, the optical section will need to be replaced. The modular and weldless flange design of the tube greatly simplifies such replacement operations.

The instrumentation section is the final portion through which the detonation wave traverses, and is of similar stainless steel construction as the ignition section. The instrumentation section features multiple ports in fourteen locations along the outer diameter of the tube, which can be used for additional optical access for line-of-sight diagnostic techniques, such as laser absorption spectroscopy (Nair et al. 2020, 2023). Piezoelectric time-of-arrival (TOA) sensors (Dynasen, Inc.) are mounted along the top five ports—equally spaced 101.6 mm (4 in) apart—to record the wavespeed of the fully developed flow.

2.2 Soot foil method

Soot foil measurements were used as validation of the experimental chemiluminescence approach. Aluminum sheets—with 0.5 mm thickness and dimensions of 50.8 mm (2 in) × 76.2 mm (3 in)—were cut, rolled, and coated with soot, following the methods described by Crane et al. (2019) and

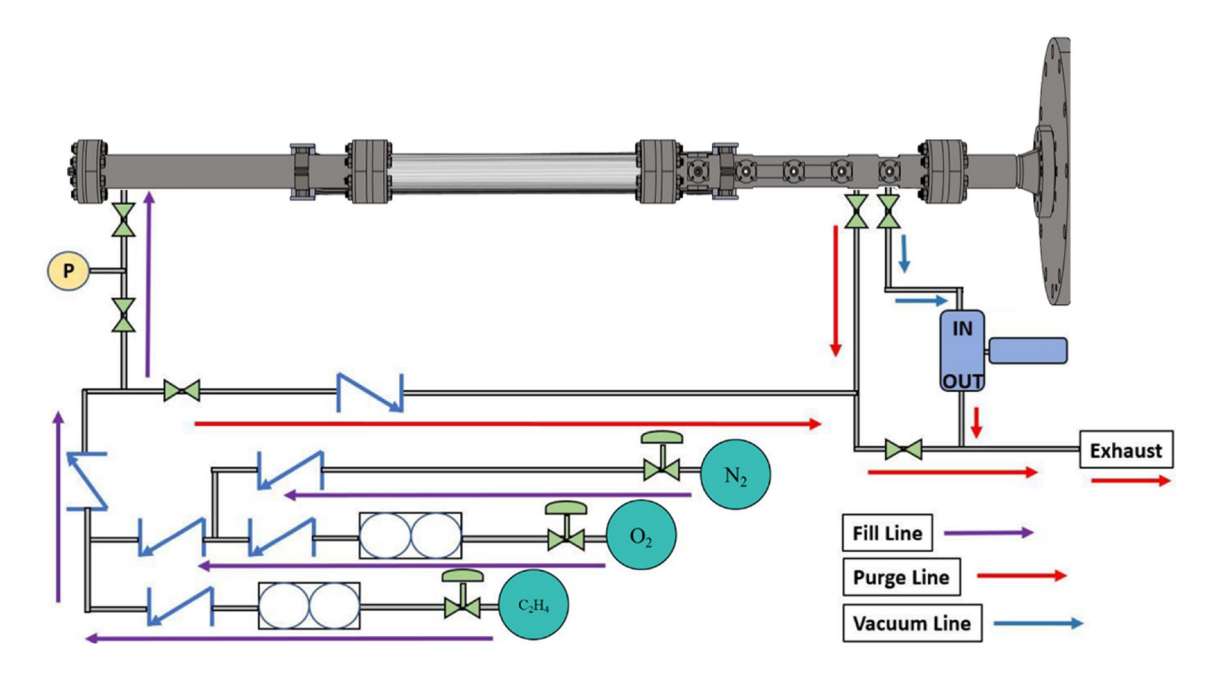


Fig. 2 Schematic of the optically accessible detonation tube and gas manifold



108 Page 4 of 10 Experiments in Fluids (2024) 65:108

Shi et al. (2021). Aluminum sheets were chosen for their relative rigidity, as thinner and lighter materials would be swept into the vacuum tank upon passage of a detonation wave. A soot-coated sheet was placed downstream of the visual section at the end of the detonation tube for each test run. Caution was taken to ensure the sheets held against the tube walls and sat as flush as possible within the channel to mitigate intrusion into the flow. After each detonation, the sheets were carefully removed, flattened and photographed with a 12 megapixel camera (3024 \times 4032 pixel resolution). Each sheet was photographed with a ruler alongside its straight edge for spatial calibration, which typically resulted in a scaling of 40 pixels/mm.

2.3 CH* chemiluminescence optical setup

The chemiluminescence imaging setup comprised a single high-speed camera (Photron SA-Z) outfitted with a 60-mm Nikon lens (f/4) and a 430-nm narrow-bandpass filter (10 nm FWHM, Edmund Optics), chosen to target CH* emission, fixed between the camera lens and acrylic tube. A simplified diagram of the optical configuration is illustrated in Fig. 3.

Images were captured at a rate of 100,000 frames per second with an exposure time of 6250 ns and a resolution of 640×280 pixels. Notably, the implementation presented in this work uses a global shutter, which mitigates directional distortion of the chemiluminescence produced by a traveling detonation wave while also capturing the path of the triple point in a single image, as depicted in Fig. 1. Implementations using a rolling shutter may enable lower exposure times at the expense of horizontal directional row-by-row distortion in the final image. The camera's focusing lens was adjusted to view the flow directly in the center of the tube. It was found that the cylindrical geometry of the acrylic tube did not noticeably distort the captured images when focused

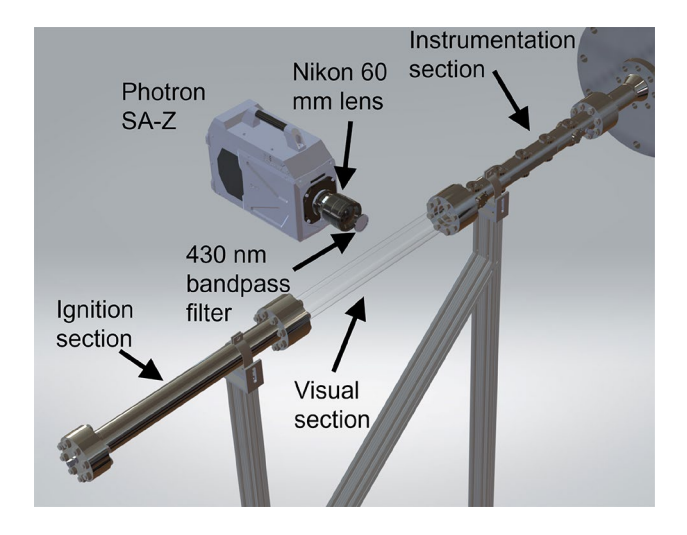


Fig. 3 Rendering of the detonation tube facility and optical setup



on the center plane of the channel for the field-of-view in the configuration used in this study; this was verified by comparing spatial calibration images in which photos were taken of a ruler at two different locations—above the acrylic tube and within the detonation channel. Both instances produced the same scaling of 18 pixels/mm, confirming minimal distortion in the imaging system. This scaling also translates to a field-of-view of approximately 35.56 mm × 15.56 mm.

2.4 Data processing

Cell size for both soot foil images and chemiluminescence images were each determined by two methods: (1) manual measurement of individual cells and (2) spectral analysis. Both of these methods are described here in this subsection.

The first method to determine detonation cell size involved manually processing the images in the computer application ImageJ[™] (Schneider et al. 2012). Soot foil images for each experiment—organized by initial pressure condition-were gray-scaled and contrast was enhanced so that the cellular patterns appeared more prominently. The line tool in ImageJTM was used to measure the cell size in terms of pixels from a population of at least ten different cells. These measurements were converted to millimeters with the previously determined scaling values and averaged to determine the mean cell size for each initial pressure condition. For the corresponding chemiluminescence image for each detonation, a slightly different processing approach was used due to the relatively higher pixel intensities in the images and line-of-sight measurement which obfuscated manually identifying triple points and shocks in a consistent manner. Figure 4 depicts the approach used for enhancement of the chemiluminescence images. The raw chemiluminescence image was overlaid with a false color map ("gem" option located in the ImageJTM lookup table function) and a fast Fourier transform (FFT) bandpass filter was applied to the color-mapped image. This process filters out the high frequency or larger structures within the image—in this case, the relatively low luminous zones between the transverse waves. The final processed image (Fig. 4) accentuates the relatively high luminosity along the transverse waves, corresponding to the triple-point intersections depicted in Fig. 1. The line tool was then used to measure prominent cell sizes in terms of pixels and converted to millimeters, after which the measured cell sizes were then averaged.

The second method to determine cell size involved spectral analysis of each image. A digital image processing MATLAB package developed by Hébral and Shepherd (2007) was employed to spectrally analyze both the soot foil and chemiluminescence images. The script was originally created to offer a systematic way to determine DCS from soot foil images in a repeatable and objective manner independent of the user, as manual measurements may

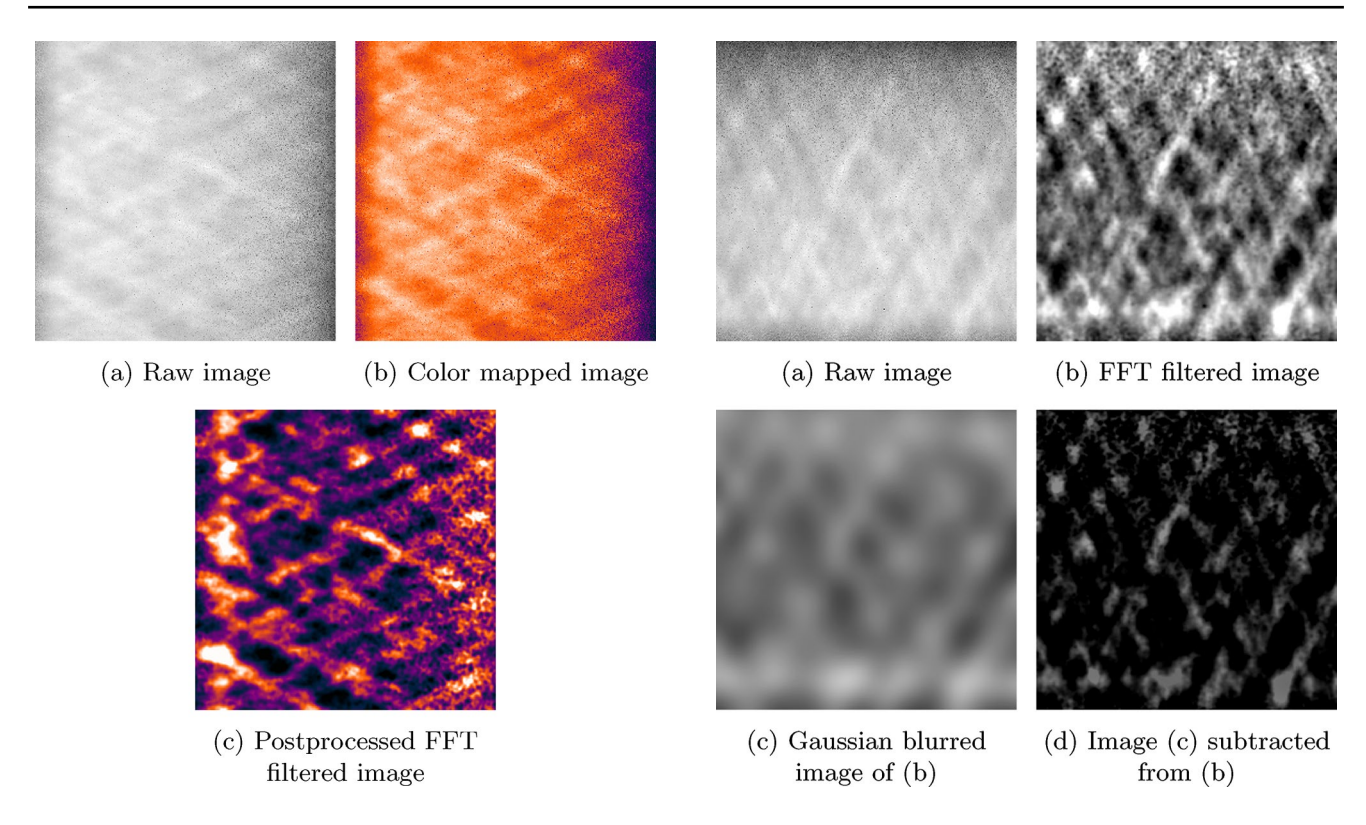


Fig. 4 Chemiluminescence image processing for manual measurements of detonation cell size

Fig. 5 Chemiluminescence image processing for spectral analysis of detonation cell size

result in uncertainties of \pm 50% or even greater, especially with the inherent irregularity of patterns created by certain mixtures (Hébral and Shepherd 2007). The basis of the technique involves computing a two-dimensional Fourier analysis to highlight the fundamental spatial frequencies in the cellular patterns and their harmonics. As part of the image processing, edge detection is used to emphasize the cellular pattern, and a power spectral density (PSD) calculation is made. The PSD is used to extract the fundamental frequency and its harmonics. The soot foil images were gray-scaled in ImageJTM as previously and cropped to a typical 280×280 pixel resolution, since a square image is recommended by Hébral and Shepherd (2007) for optimal processing. Each image is duplicated, after which a Gaussian blur was applied. Image subtraction was performed on the original image by the blurred image to obtain an image with reduced uneven lighting and uniform pixel values. The resulting images were rotated so that the propagation direction was vertical, as the MATLAB script was written to process images assuming detonation cell widths in the horizontal direction. The images were subsequently processed through the MATLAB script to obtain the dominant spatial frequency and, thus, cell size.

For the spectral analysis in this work, the chemiluminescence images required slightly different preprocessing. The method described is outlined in Fig. 5. An FFT bandpass

filter was applied to the cropped, raw chemiluminescence images so that the high-frequency luminous zones were attenuated or removed (Fig. 5). Since FFT-based image analyses group similar spatial frequencies together on the power density spectrum, out-of-plane triple-point paths captured within the three-dimensional field—which can convolute manually discerned analyses—are also included in the spectrally based detonation cell size analysis. A duplicate image was created with a Gaussian blur (Fig. 5) as was performed with the soot foil images. Image subtraction of the blurred image from the original image was then performed (Fig. 5). The resulting image was then processed through the MATLAB script.

3 Results

Cell sizes for both soot foil and chemiluminescence images were first determined by manual measurements through the ImageJTM software. The average measured cell sizes are plotted in Fig. 6 on an inverse scale $(1/\lambda)$ versus initial pressure conditions, and are compared with experimental soot foil measurements from three previous studies (Abid et al. 1993; Strehlow and Engel 1969; Knystautas et al. 1982). These prior experimental data are sourced from the Caltech detonation database (Shepherd 2005). Each of the previous



108 Page 6 of 10 Experiments in Fluids (2024) 65:108

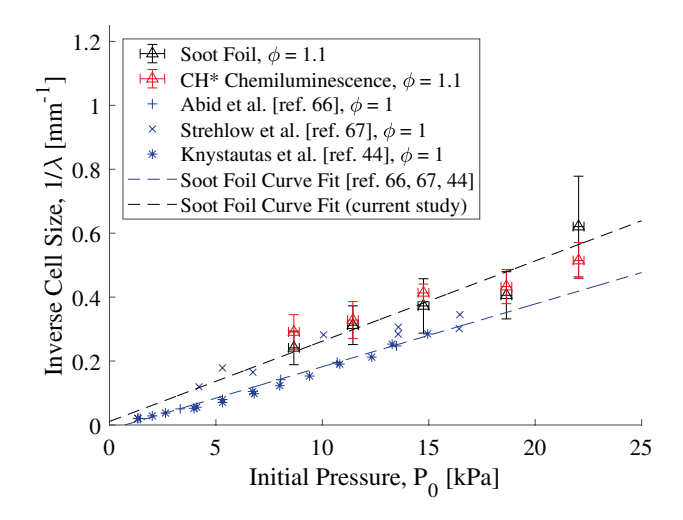


Fig. 6 Manually determined detonation cell size compared with previous studies from the Caltech database across initial pressure conditions

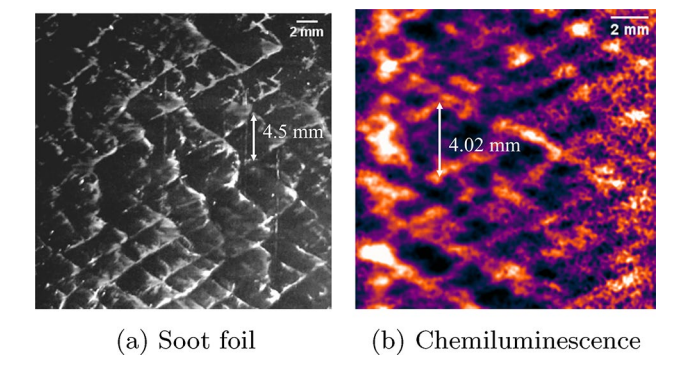


Fig. 7 Soot foil and chemiluminescence comparison of the cellular structure of C_2H_4 - O_2 detonation waves at P_0 = 11.43 kPa and ϕ = 1.1

studies includes detonations with stoichiometric ($\phi=1.0$) C_2H_4 - O_2 at various initial pressure conditions. Linear regressions were applied to both the soot foil data collected in the present work and the aggregate data from the literature, and error bars are plotted (calculated as one standard deviation—within a 68% confidence interval) with the data of the current study. The linear regressions correlate consistently with each other, although the measurements of the current study highlight the overall smaller cell size as a result of the fuel-rich mixtures. This, however, is expected as fuel-rich mixtures in this regime are known to produce smaller cell sizes (Batraev et al. 2018).

Figure 7 compares the filtered chemiluminescence image of $P_0 = 11.43$ kPa and its corresponding soot foil record. The images are annotated with the cell width of single chosen cells to demonstrate the relative agreement between the two measurement methods. To visually communicate the effect

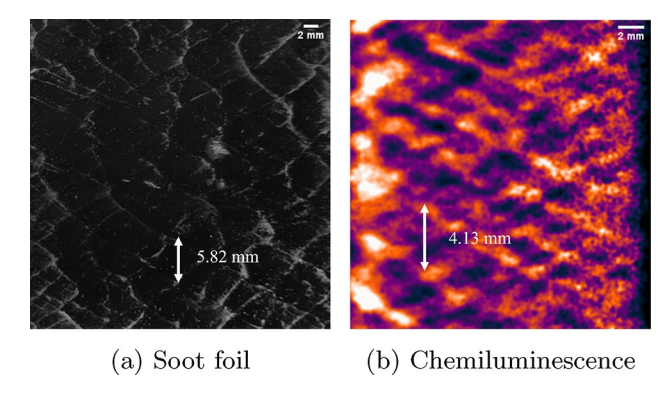


Fig. 8 Soot foil and chemiluminescence comparison of the cellular structure of C_2H_4 – O_2 detonation waves at $P_0 = 8.66$ kPa and $\phi = 1.1$

Table 1 Average measured soot foil and chemiluminescence cell size

$\overline{P_0 \text{ (kPa)}}$	λ_{soot} (mm)	$\lambda_{\mathrm{CH}*} (\mathrm{mm})$	Diff. (%)
8.66	4.14	3.44	17.04
11.43	3.20	3.05	4.87
14.75	2.71	2.42	10.61
18.65	2.46	2.31	6.27
22.04	1.61	1.94	20.68

of pressure, another filtered chemiluminescence image of a detonation with $P_0 = 8.66$ kPa and its corresponding soot foil record are shown in Fig. 8, displaying slightly larger cell sizes. The average measured cell size for the two methods is tabulated in Table 1 for all other initial pressures. Percent difference is also determined with the soot foil record treated as the expected value, and the chemiluminescence as the observed value.

Cell size was also determined by spectral analysis to ascertain measurements more objectively. Preprocessed images of both soot foil and chemiluminescence were processed using MATLAB scripts developed by Hébral and Shepherd, as discussed previously. Final output resulted in the fundamental spatial frequency of each image and its associated harmonics. Relative energies of the harmonics are also computed to determine the dominant spatial frequency, which effectively indicates the dominant cell size. Table 2 shows the dominant cell size for each soot foil and chemiluminescence image at each initial pressure.

Percent error is calculated in the same manner as previously, with traditional soot foil treated as an expected value and chemiluminescence treated as an observed value. Notably, the percent deviations are significantly lower than those determined using manual measurements. Figure 9 plots the manually measured cell sizes alongside the automatically computed cell sizes as a function of initial mixture pressure. It can be seen that there is little



Table 2 Soot foil and chemiluminescence cell size determined by spectral analysis

P_0 (kPa)	$\lambda_{\rm soot}$ (mm)	$\lambda_{\mathrm{CH}*}$ (mm)	Diff. (%)
8.66	4.08	3.77	7.53
11.43	3.00	3.38	12.45
14.75	2.75	2.42	12.06
18.65	2.68	2.78	3.81
22.04	1.52	1.58	3.68

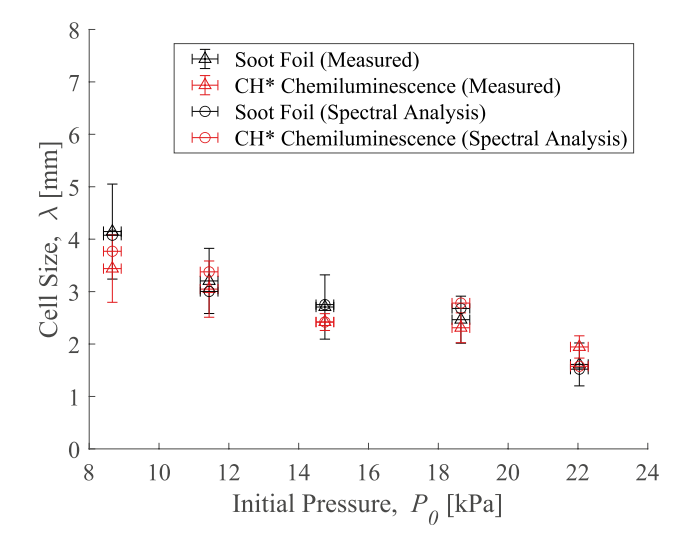


Fig. 9 Detonation cell size comparison between manual measurements and spectral analysis

deviation between any set of measurements for a given initial pressure. In certain cases, soot foil and chemiluminescence cell size are nearly the same, such as for P_0 = 18.65 kPa where there is little difference between sets of measurements determined by the same method (i.e., by manual measurement or spectral analysis). In another case such as for P_0 = 14.75 kPa, cell sizes for the same measurement technique (i.e., by soot foil or chemiluminescence) are effectively the same.

Lastly, the current study's experimental soot foil data is compared to Caltech detonation database data in terms of theoretical induction length Δ_i —a length parameter associated with the reactivity of a mixture—to further compare the trends observed by others in previous investigations of detonative mixtures. Detonation cell size for various hydrocarbon fuels detonated with air or oxygen are also obtained from the database and referenced from Nair et al. (2023). The data comprise stoichiometric mixtures of various hydrocarbon fuels with initial pressure conditions of nominally 1 atm. Induction length is simulated using the Caltech Shock and Detonation Toolbox (Goodwin et al. 2018) in Canternal (Browne et al. 2008). The data are plotted in Fig. 10.

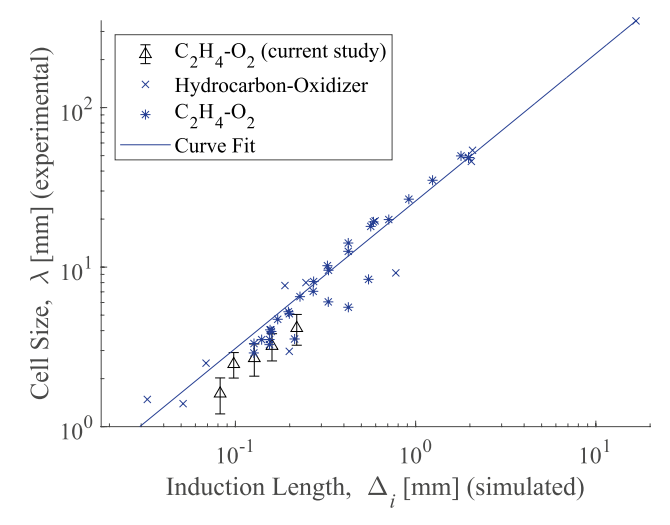


Fig. 10 Experimental detonation cell size versus simulated detonation induction length for hydrocarbon-oxidizer mixtures

A curve fit is also plotted as a power law, relating cell sizes and induction length:

$$\lambda = 25.96(\Delta_z)^{0.9239}$$

4 Discussion

The determination of detonation cell size from soot foil measurements has historically involved subjective human measurement, which has been mitigated via spectral analysis of soot foil-based measurements (Hébral and Shepherd 2007); this work aims to expand these spectral techniques to chemiluminescence-based measurements, and here we discuss some associated challenges with doing so.

For the measured detonation cell sizes, a potential source of error is attributed not only to the subjective determination of the triple points, but to the line-of-sight nature of chemiluminescence and depth of field of the optical setup although the high-speed camera lens was focused in the center plane of the detonation channel, there is a limitation in discerning depth details, as discussed by Fugger et al. (2020). Luminosity associated with out-of-plane transverse waves could obfuscate the in-plane waves, enlarging areas of high luminosity or making areas more diffuse. That is, luminosity from the out-of-plane waves may be superimposed on the in-plane transverse spacings (within the cells), obfuscating triple-point paths and possibly skewing measurements. Relatedly, for very low initial pressure conditions—wherein the detonation cell size is very sensitive to initial pressure slightly higher pressures in the boundary layer (where soot



foil measurements are typically recorded) could possibly produce smaller cell sizes than in the core flow, generating out-of-plane waves in the chemiluminescence images possessing multiple cell sizes. However, for the conditions examined in this work, the cell size data do not indicate this behavior.

Unburned pockets of reactants could also produce chemiluminescence not associated with the detonation cellular structure (Lemcherfi et al. 2023). These can be seen in the filtered chemiluminescence images (such as in Figs. 4 and 5) where luminosity exists considerably despite the attenuation of the transverse spacings through bandpass filtering. Nonetheless, for the undiluted near-stoichiometric ethylene/oxygen mixtures investigated with initial pressures ranging from 8 to 22 kPa, the spectral analysis approach to estimating detonation cell size is shown to be robust against these artifacts in the chemiluminescence images. At pressures higher than 22 kPa, the out-of-plane luminosity was observed to be too significant to reliably discern the paths of individual triple-point intersections, precluding estimations of detonation cell size for the available exposure times of the Photron SA-Z using a global shutter.

The attenuation provided by the filtering process is also less effective as initial reactant fill pressure increases, since luminosity is expected to increase from the increase in molecular concentration and associated increase in chemiluminescence events. This reduces the clarity of the chemiluminescencebased image relative to the traditional soot foil-based method, which can retain much sharper features—such as shown in Fig. 7—however; the reduced turnaround time of the chemiluminescence-based may still be attractive to some researchers for these detonation conditions. Figure 11 shows the pixel intensity profiles of two raw chemiluminescence images from detonation experiments with two different initial fill pressures. The detonations propagate from left to right, and the intensity profiles are taken from left to right of each image. As expected for both profiles, the highest luminosity is seen downstream (left) where the most recent reactions are captured, and luminosity decays further upstream of the image (right). For the mixture at the higher initial fill pressure, luminosity is less uniform and much greater than that of the mixture at the lower initial fill pressure. It can be inferred that increasing pressure will produce more intense pixel values (luminosity) and more diffuse regions. For the Photron SA-Z camera used in the study, saturation occurs at a pixel value of 4095 (16bit images). Although the highest initial pressure recorded in this study did not cause saturation or oversaturation, it is still noteworthy to consider the effects, as areas of saturation/oversaturation in images are difficult to use in digital image processing largely owing to the 'pixels/mm' window resolution in our current optical configuration—in some cases images may be completely unusable. For the optical setup and data presented here and considering these effects, we can only estimate

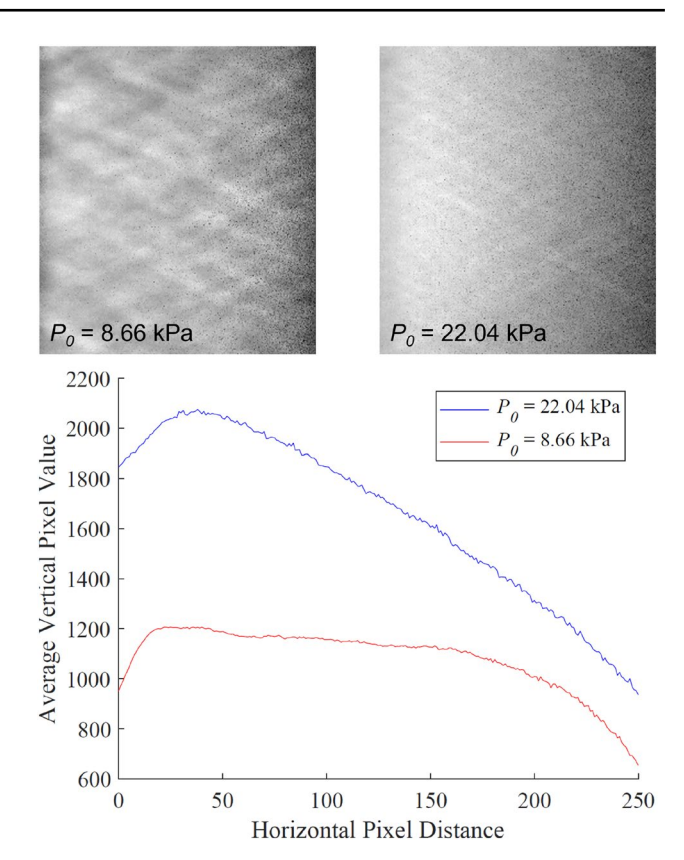


Fig. 11 Pixel intensity profiles of raw chemiluminescence images at $P_0 = 8.66$ kPa and $P_0 = 22.04$ kPa

that the lower limit of resolvable cell size of this technique is that of our smallest measured cell size (1.6 mm), although smaller cell sizes may be resolvable with lenses possessing increased magnification power. For extended applications of the chemiluminescence-based approach presented here, it is anticipated that higher initial fill pressures will require greater camera resolution to resolve the detonation structures and/or adjustments to the optical setup to prevent oversaturation.

Lastly, we should note that since the technique presented here is based on chemiluminescence of CH* produced by carbon-containing fuels, it is expected to be less effective in measuring detonation cell sizes in fuel-lean mixtures and more effective in fuel-rich mixtures for the range of initial pressures presented. Moreover, the technique explored in this work is not applicable to fuels comprising only nitrogen and/or hydrogen atoms, for which established OH* chemiluminescence techniques are better suited.

5 Summary and conclusions

Detonation cell sizes from five distinct detonations are reported from experiments enabled by an optically accessible linear detonation tube using undiluted mixtures of



gaseous ethylene and oxygen at initial fill pressures up to 22 kPa. Simultaneous soot foil measurements and CH* chemiluminescence images were recorded to quantitatively assess detonation cell size, down to 1.6 mm in width. Specifically, long-exposure CH* chemiluminescence imaging at 100 kHz enabled by the optically accessible section of the detonation tube revealed the spatial histories of the interacting shock waves comprising the detonation wave fronts. The resulting chemiluminescence images are analogous to traditional soot foil methods, wherein the detonation wave front and structure are traced, and may be considered 'optical soot foils' (Fugger et al. 2020). To the authors' knowledge, this is the first direct comparison of these two detonation cell size measurement methods recorded simultaneously within the same controlled detonation experiments.

Manual measurement of the soot foil records and their corresponding chemiluminescence images showed excellent agreement. The experimentally measured cell sizes were compared to known cell size data from previous studies in the literature which were sourced from the Caltech detonation database. Linear regressions of the data indicate that the results of previous studies and the current experimental data are reasonably consistent with each other. To overcome convolutions posed by the line-of-sight nature of chemiluminescence imaging, cell sizes from the soot foil and chemiluminescence images were also determined by spectral analysis. The soot foil and chemiluminescence-based methods agreed with one another more closely than when manually measuring the detonation cell sizes. When compared to their corresponding manually determined measurements, the spectrally analyzed measurements were still consistent and agreed within measurement uncertainty. Little deviation was observed and, in some cases, results yielded the same functional cell size within measurement uncertainty.

The use of CH* chemiluminescence as a method to passively determine detonation cell size shows high promise, especially when resulting measurements are in good agreement with those provided by the more labor-intensive traditional soot foil method. However, limitations of the approach are noted, namely for detonations through mixtures at higher initial fill pressures, wherein diffuse and intense luminosity may cause oversaturation or make triple points indiscernible. Chemiluminescence may also vary for different reactant mixtures with varying C/H atomic ratios and require adjustments to the optical setup initially described in this work. Nonetheless, for experiments that can employ this approach, detonation cell size may reliably be optically estimated, and expands the potential for time-resolved measurements of detonation cell size in optically accessible, continuously operating devices which may have non-uniform propellant mixtures (Fugger et al. 2020).

Acknowledgements The authors thank Dean Kaialau for the design and construction of the detonation tube at UTSA, Anil P. Nair and Joseph Hernandez-McCloskey for valuable input during the design of the UTSA detonation tube, and Elijah LaLonde for experimental testing assistance at UTSA. Additionally, the authors thank Prof. Xian Shi (University of California, Irvine) for helpful advice on performing soot foil measurements in detonation channels.

Author contributions BMN wrote the main manuscript text and generated and analyzed the experimental data and diagrams presented in all of the figures. ENH assisted with the experiments and data collection. DIP edited the main manuscript text, performed simulations for Fig. 10, and provided funding for the project. CSC provided funding for the project. All authors reviewed the manuscript.

Funding This work is supported in part by the US Air Force Office of Scientific Research (AFOSR), Grant No. FA9550-17-1-031, with Chiping Li as Program Officer, and the US National Aeronautics and Space Administration (NASA), Grant. No. 80NSSC19M0194, the US National Science Foundation (NSF), Award No. 2135789, and The American Chemical Society Petroleum Research Fund (ACS-PRF), Doctoral New Investigator Grant No. 65560-DNI6.

Data availability The data that support the findings of this study are available from the corresponding author, DIP, upon reasonable request.

Declarations

Competing interests The authors declare no competing interests.

Ethical approval and consent to publish All authors consented to publication of this manuscript.

References

Abid S, Dupre G, Paillard C (1993) Oxidation of gaseous unsymmetrical dimethylhydrazine at high temperatures and detonation of UDMH/O₂ mixtures. In: Dynamic aspects of detonations, pp 162–181. American Institute of Aeronautics and Astronautics, Washington. https://doi.org/10.2514/5.9781600866265.0162.0181

Athmanathan V, Braun J, Ayers ZM, Fugger CA, Webb AM, Slip-chenko MN, Paniagua G, Roy S, Meyer TR (2022) On the effects of reactant stratification and wall curvature in non-premixed rotating detonation combustors. Combust Flame 240:112013. https://doi.org/10.1016/j.combustflame.2022.112013

Aul CJ, Metcalfe WK, Burke SM, Curran HJ, Petersen EL (2013) Ignition and kinetic modeling of methane and ethane fuel blends with oxygen: a design of experiments approach. Combust Flame 160(7):1153–1167. https://doi.org/10.1016/j.combustflame.2013. 01.019

Ayers ZM, Lemcherfi A, Plaehn EW, Gejji RM, Perkins HD, Roy S, Slabaugh CD, Meyer TR, Fugger CA (2022) Simultaneous 100-kHz acetone planar laser-induced fluorescence and OH* chemiluminescence in a linear non-premixed detonation channel. Combust Flame 244:112209. https://doi.org/10.1016/j.combustflame.2022.

Batraev IS, Vasil'ev AA, Ul'yanitskii VY, Shtertser AA, Rybin DK (2018) Investigation of gas detonation in over-rich mixtures of hydrocarbons with oxygen. Combust Explos Shock Waves 54(2):207–215. https://doi.org/10.1134/S0010508218020107

Bennewitz JW, Bigler BR, Schumaker SA, Hargus WA (2019) Automated image processing method to quantify rotating detonation wave behavior. Rev Sci Instrum 10(1063/1):5067256



- Browne S, Ziegler J, Shepherd JE (2008) Numerical solution methods for shock and detonation jump conditions. GALCIT Report FM2006.006 (July 2004)
- Cadman P, Bambrey RJ, Box SK, Thomas GO (2002) Ethylene combustion studied over a wide temperature range in high-temperature shock waves. Combust Sci Technol 174(11–12):111–127. https://doi.org/10.1080/713712958
- Chatelain KP, Rojas Chavez SB, Vargas J, Lacoste DA (2023) Towards laser-induced fluorescence of nitric oxide in detonation. Shock Waves 33(3):179–189. https://doi.org/10.1007/ s00193-023-01134-5
- Crane J, Shi X, Singh AV, Tao Y, Wang H (2019) Isolating the effect of induction length on detonation structure: hydrogen—oxygen detonation promoted by ozone. Combust Flame 200:44–52. https:// doi.org/10.1016/j.combustflame.2018.11.008
- Frederick MD, Gejji RM, Shepherd JE, Slabaugh CD (2022) Time-resolved imaging of the cellular structure of methane and natural gas detonations. Shock Waves 32(4):337–351. https://doi.org/10.1007/s00193-022-01080-8
- Frederick MD, Gejji RM, Shepherd JE, Slabaugh CD (2023) Statistical analysis of detonation wave structure. Proc Combust Inst 39(3):2847–2854. https://doi.org/10.1016/j.proci.2022.08.054
- Fugger CA, Cho KY, Hoke J, Gomez Gomez M, Meyer TR, Schumaker SA, Caswell AW (2020) Detonation dynamics visualization from megahertz imaging. In: AIAA Scitech 2020 forum. American Institute of Aeronautics and Astronautics, Reston, Virginia. https://doi.org/10.2514/6.2020-0441
- Goodwin DG, Moffat HK, Speth RL (2018) Cantera: an object-oriented software toolkit for chemical kinetics, thermodynamics, and transport processes . https://doi.org/10.5281/zenodo.170284
- Gray JAT, Lacoste DA (2021) Effect of the plasma location on the deflagration-to-detonation transition of a hydrogen-air flame enhanced by nanosecond repetitively pulsed discharges. Proc Combust Inst 38(3):3463–3472. https://doi.org/10.1016/j.proci. 2020.06.369
- Hébral J-P, Shepherd JE (2007) Spectral analysis for cell size measurement. https://shepherd.caltech.edu/EDL/PublicResources/CellImageProcessing/cellsize.html
- Heiser WH, Pratt DT (2008) Thermodynamic cycle analysis of pulse detonation engines. J Propuls Power 18(1):68–76. https://doi.org/10.2514/2.5899
- Kaneshige M, Shepherd JE (1997) Detonation database. Technical Report FM97-8, GALCIT. http://www.galcit.caltech.edu/detn_db/html/
- Kellenberger M, Ciccarelli G (2015) Propagation mechanisms of supersonic combustion waves. Proc Combust Inst 35(2):2109–2116. https://doi.org/10.1016/j.proci.2014.08.002
- Knystautas R, Lee JH, Guirao CM (1982) The critical tube diameter for detonation failure in hydrocarbon-air mixtures. Combust Flame. https://doi.org/10.1016/0010-2180(82)90116-X
- Lee JHS (2008) The detonation phenomenon. Cambridge University Press
- Lemcherfi A, Gejji RM, Ayers ZM, Plaehn EW, Perkins HD, Roy S, Meyer TR, Fugger CA, Slabaugh CD (2023) Effect of injection dynamics on detonation wave propagation in a linear detonation combustor. Proc Combust Inst 39(3):2875–2883. https://doi.org/ 10.1016/j.proci.2022.08.004
- Liu Y, Tan J, Wan M, Zhang L, Yao X (2020) Quantitative measurement of OH and CH chemiluminescence in jet diffusion flames.

- ACS Omega 5(26):15922–15930. https://doi.org/10.1021/acsomega.0c01093
- Lu FK, Braun EM (2014) Rotating detonation wave propulsion: experimental challenges, modeling, and engine concepts. J Propuls Power 30(5):1125–1142. https://doi.org/10.2514/1.b34802
- Nair AP, Jelloian C, Morrow DS, Bendana FA, Pineda DI, Spearrin RM (2020) MHz mid-infrared laser absorption sensor for carbon monoxide and temperature behind detonation waves. In: AIAA Scitech 2020 forum. American Institute of Aeronautics and Astronautics, Reston, Virginia, https://doi.org/10.2514/6.2020-0733
- Nair AP, Keller AR, Minesi NQ, Pineda DI, Spearrin RM (2023) Detonation cell size of liquid hypergolic propellants: estimation from a non-premixed combustor. Proc Combust Inst 39(3):2757–2765. https://doi.org/10.1016/j.proci.2022.06.015
- Nair AP, Minesi NQ, Kuenning NM, Keller AR, Spearrin RM (2023) Optical pressure sensing at MHz rates via collisional line broadening of carbon monoxide: uncertainty quantification in reacting flows. Appl Phys B 129(4):51. https://doi.org/10.1007/s00340-023-07985-1
- New TH, Panicked PK, Lu FK, Tsai HM (2006) Experimental investigations on DDT enhancements by shchelkin spirals in a PDE. In: Collection of technical papers—44th AIAA aerospace sciences meeting, vol 9, no January, pp 6674–6683. https://doi.org/10.2514/6.2006-552
- Radulesco MI, Sharpe GJ, Law CK, Lee JHS (2007) The hydrodynamic structure of unstable cellular detonations. J Fluid Mech 580:31–81. https://doi.org/10.1017/S0022112007005046
- Rankin BA, Richardson DR, Caswell AW, Naples AG, Hoke JL, Schauer FR (2017) Chemiluminescence imaging of an optically accessible non-premixed rotating detonation engine. Combust Flame 176:12–22. https://doi.org/10.1016/j.combustflame.2016. 09.020
- Rojas Chavez SB, Chatelain KP, Lacoste DA (2023) Induction zone length measurements by laser-induced fluorescence of nitric oxide in hydrogen-air detonations. Proc Combust Inst 39(3):2885–2894. https://doi.org/10.1016/j.proci.2022.09.020
- Schneider CA, Rasband WS, Eliceiri KW (2012) NIH Image to ImageJ: 25 years of image analysis . https://doi.org/10.1038/nmeth.2089
- Shi X, Crane J, Wang H (2021) Detonation and its limit in small tubes with ozone sensitization. Proc Combust Inst 38(3):3547–3554. https://doi.org/10.1016/j.proci.2020.06.133
- Strehlow RA, Engel CD (1969) Transverse waves in detonations. II. Structure and spacing in H₂-O₂, C₂H₄-O₂, and CH₄-O₂ systems. AIAA J 7(3):492–496. https://doi.org/10.2514/3.5134
- Wolański P (2013) Detonative propulsion. Proc Combust Inst 34(1):125–158. https://doi.org/10.1016/j.proci.2012.10.005
- Zhang F (ed) (2012) Shock waves science and technology library, vol 6. Springer, Berlin. https://doi.org/10.1007/978-3-642-22967-1

Publisher's Note Springer Nature remains neutral with regard to jurisdictional claims in published maps and institutional affiliations.

Springer Nature or its licensor (e.g. a society or other partner) holds exclusive rights to this article under a publishing agreement with the author(s) or other rightsholder(s); author self-archiving of the accepted manuscript version of this article is solely governed by the terms of such publishing agreement and applicable law.

